Modeling the biodiesel production using the wheat straw ash as a catalyst

Ana Veličković[1], Jelena Avramović[1], Milan Kostić[2], Jugoslav B. Krstić[3], Olivera Stamenković[2] i Vlada B. Veljković[2,4,]

[1]*University in Priština - Kosovska Mitrovica, Faculty of Technical Sciences, Knjaza Miloša 7, 38220, Serbia*
[2]*Faculty of Technology, University of Niš, Bulevar oslobođenja, 16000 Leskovac, Serbia*
[3]*University of Belgrade – Institute of Chemistry, Technology and Metallurgy, Belgrade, Serbia*
[4]*The Serbian Academy of Sciences and Arts, Knez Mihailova 35, 11000 Belgrade, Serbia*

Abstract

Wheat straw ash (WSA) was investigated as a new catalyst in biodiesel production from sunflower oil. The catalyst was characterized by temperature-programmed decomposition, X-ray powder diffraction, Hg porosimetry, N_2 physisorption, and scanning electron microscopy - energy dispersive X-ray spectroscopy methods. The methanolysis reaction was tested in the temperature range of 55–65 ^{o}C, the catalyst loading range 10–20 % of the oil weight, and the methanol-to-oil molar ratio range 18 : 1–24 : 1. The reaction conditions of the sunflower oil methanolysis over WSA were optimized by using the response surface methodology in combination with the historical experimental design. The optimum process conditions ensuring the highest fatty acid methyl esters (FAME) content of 98.6 % were the reaction temperature of 60.3 ^{o}C, the catalyst loading of 11.6 % (based on the oil weight), the methanol-to-oil molar ratio of 18.3 :1, and the reaction time of 124 min. The values of the statistical criteria, such as coefficients of determination (R^2 = 0.811, R^2_{pred} = 0.789, R^2_{adj} = 0.761) and the mean relative percent deviation (MRPD) value of 10.6 % (66 data) implied the acceptability and precision of the developed model. The FAME content after 4 h of reaction under the optimal conditions decreased to 37, 12, and 3 %, after the first, second, and third reuse, respectively.

keywords: agricultural residues; fatty acid methyl esters; catalyst characterization; model; optimization.

Available on-line at the Journal web address: http://www.ache.org.rs/HI/

1. INTRODUCTION

Given the growing global need for energy and the scarcity of fossil fuel reserves, as well as the severe climate change, the question is imposed of future energy sources that will be able to meet the need of the economy and society. Therefore, the emphasis must be put on renewable and sustainable energy sources, such as biomass, solar, wind, and geothermal energy. Biomass including waste agricultural residues is significant as a source for energy production by combustion or for biofuel production *via* various chemical, biological, or thermochemical routes. Recently, it has been estimated that about 3–14 % of the total energy supply in the world could be generated from agricultural residues [1].

Biodiesel, a biomass-based fuel, is commonly produced by chemical conversion of vegetable oils, and widely used as an adequate replacement for diesel fuel. The advantages of biodiesel, compared to petroleum-based diesel, are renewability, sustainability, and reduced emission of CO_2, SO_2, and hydrocarbons [2].

Heterogeneous catalysts (metal oxides, mixed oxides, supported alkali metals, zeolites, hydrotalcites, etc.) have been investigated as more favorable options than homogeneous ones for they are less corrosive, more environmentally friendly, easily separable, and potentially reusable [2-4]. To enhance the overall sustainability of the biodiesel

production process and to reduce the production costs, the attention of researchers has been recently directed towards low-cost ashes as heterogeneous catalysts. These materials are derived by combusting high volume resources, such as agricultural biomass including plant residues from the crop, fruit, and viticulture production [5]. The advantages of waste biomass are wide availability, low price, sustainability, and renewability. Besides providing a highly active catalyst for biodiesel production, this approach is both cost-effective and eco-friendly.

In recent years, many researchers have combusted different biomass materials, specific for each climate region, to get ashes, which have been successfully employed as efficient catalysts in biodiesel production. A review of the ash-based catalysts used in biodiesel production is given in Table 1.

Table 1. A review of agricultural waste-based ashes catalysts used in biodiesel production

Source of catalyst	Active species	Oil source	Methanol/oil molar ratio	Catalyst loading, %	t / °C	Ester yield (content), % / min	Statistical method[d]	Ref.
Musa paradisiacal peels	K	*Azadirachta indica*	16.74:1	0.65	65	99.2/57	3⁵ CCD	[6]
Musa paradisiacal peels	K	*Thevetia peruviana*	6.85:1	3	60	95/90	Box–Behnken + ANN	[7]
Banana peels	-	Palm kernel	14.63:1	4	65	99.5/65	3⁵ CCD	[8]
	K	*Bauhinia monandra*	6.86:1	2.75	65	98.5/69	2³ CCD	[9]
Musa balbisiana Colla peel	K	Waste cooking (WCO)	6:1	2	60	100/180	-	[10]
Tucuma peels (Astrocaryum aculeatum Meyer*)*	K	Soybean oil	15:1	1	80	97.3/240	-	[22]
Musa acuminata Colla 'Red' banana peduncle	K, Si, Ca, Mg	*Ceiba pentandra* (CPO)	11.5:1	2.68	65	98.73/106	CCD	[11]
Banana (*Musa spp.* 'Pisang Awak') peduncle	K	*Ceiba pentandra* (CPO)	9.2:1	1.978	60	98.69/60	CCD	[12]
Musa balbisiana stem	K, Na	*Thevetia peruviana*	10:1	20	32	96/180	-	[13]
Musa balbisiana stem	K	*Jatropha curcas*	9:1	5	275	98/60	-	[14]
Musa balbisiana underground stem	-	*Mesua ferrea*	9:1	5	275	95/60	-	[15]
Cocoa pod husk	K	*Azadirachta indica*	16.74:1	0.65	65	99/57	CCD	[16]
Cocoa pod husk	-	Palm kernel	14.63:1	4	65	99.3/65	3⁵ CCD	[8]
Coconut husk	K	Jatropha	12:1	7	45	(99.86)/45	-	[17]
Rice husk	Li, Na, K*	Used cooking	9:1	3	65	(98.2)/60	-	[18]
Walnut shell	K, Ca	Sunflower	12:1	5	60	(>98)/10	-	[19]
Palm kernel shell biochar	Ca	Sunflower	9:1	3	65	(99)/240	3³ FFD	[20]
Mangifera indica peel	K	Soybean oil	6:1	6	28	98/360	-	[21]
Birch bark	-	Palm	12:1	3	60	(88.06)/180	-	[23]
Moringa leaves ash	-	Soybean oil	6:1	6	65	86.7/120	-	[24]
Pineapple (Ananás comosus) leaves ash	K, Ca	Soybean oil	40:1	4	60	>98/30	-	[25]
Brassica nigra plant	K	Soybean	12:1	7	65	98.79/25	-	[26]
					32	98.87/75	-	
		Jatropha			65	98.26/30	-	
		Thevetia peruvianal			65	97.78/25	-	
Corn cobs	-	Corn germs	9.4:1	19.8	60	(98.1)/31	3³ FFD	[27]
Arecanut husk ash[a]	-	WCO	3:1-15:1	1-5	65	96.5/120 99.98/150	-	[28]
Citrus sinensis peel[b]	-	WCO	6:1	6	65	98/180	-	[29]
Wheat bran (ash with CaO)[c]	-	WCO	33:1	11.66	54.6	93.6/114.21	3⁵ CCD	[30]
Wheat straw	K, Si	Sunflower	18.3:1	11.6	60.3	(98.6)/124	Historical data design	This work

Supported on rice husk; [a]Ash modified with LiNO₃; [b]Ash coated Fe₃O₄ nanoparticles; [c]Ash modified with CaO from water scale from a distillation unit; [d]ANN – artificial neural network, CCD – central composite design, FFD – full factorial design.

For instance, ashes of peels from different types of bananas, were used as a catalyst for the transformation of *Azadirachta indica* [6], *Thevetia peruviana* [7], palm kernel [8], *Bauhinia monandra* [9], and waste cooking [10] oils to biodiesel. A high yield of methyl esters (> 95 %) was also obtained using ashes from other parts of banana, such as

peduncles [11,12] and stems [13-15]. Moreover, methanolysis of various oils was successfully carried out in the presence of husk ashes obtained from different biomass wastes, such as cocoa pod [8,16], coconut [17], and rice [18], walnut kernel [19] and palm kernel [20] shells, mango [21], and tucuma [22] peels ashes. Furthermore, ashes from bark [23], leaves [24,25], whole plants [26], and cobs [27] were used to catalyze biodiesel production. Some ashes were improved before the use as catalysts. Areca nut husk ash was impregnated with $LiNO_3$ to improve its alkalinity [28] while sweet orange peel ash was coated onto Fe_3O_4 nanoparticles to enhance its dispersion and stability and to enable its recovery from the reaction mixture by an external magnet [29].

Wheat straw has great potentials for many uses, such as the increase of soil fertility or the production of matting, livestock food, ethanol fuel, and heat, with the possibility of causing conflict among the potential users. Fortunately, there is enough wheat straw to be divided to fulfill all the demands, instead of being burned at fields. The yield of wheat straw during harvest is approximately 4-6 t ha^{-1} [31], depending on cutting height [32]. From a field producing 1 t of grain, 1 t of wheat straw can be harvested [33]. The annual collectible potential of wheat straw in Serbia for energy generation, calculated according to a conservative utilization rate of 30 %, is about 750,000 t [33].

In Serbia, wheat straw is the most used waste biomass for energy production by direct combustion, with average energy and ash contents of 14.4 MJ kg^{-1} and 5 %, respectively [33]. The open question related to this wheat straw utilization is what to do with the produced ash. From both the environmental and economic point of view, it should be safely treated and preferably reused in suitable production processes. The successful utilization of wheat straw ash (WSA) has been proven as a low-cost raw material in self-compacting pastes [34], a pozzolanic material in cement-based composites [35-39] and silicate glass-ceramics [40], a silica source [41,42], a filler in an alkali-activated geopolymer [43], a catalyst in char hydrogasification [44], and an adsorbent for hazardous substances removal [45-47].

This paper reports on the use of WSA as a catalyst in the production of biodiesel from sunflower oil. For a better understanding of its catalytic activity, WSA was first characterized using various techniques. Then, the reaction conditions of the sunflower oil methanolysis over WSA, like the reaction temperature, methanol-to-oil molar ratio, catalyst loading, and reaction time, were optimized using the response surface methodology (RSM) in combination with a historical experimental design. So far, there is a report of using wheat bran ashes modified with CaO obtained from water scale from a distillation unit as a catalyst [30], but according to the best knowledge of the authors, WSA has not been applied yet as a catalyst in biodiesel production. Considering the availability of wheat straw, the use of WSA as a heterogeneous catalyst could be economical.

2. MATERIALS AND METHODS

2. 1. Materials

Waste wheat straw was collected from a local farm. Edible sunflower oil (Dijamant, Zrenjanin, Serbia) was purchased in a local shopping store. The density and viscosity of the oil at 20 °C are 918.4 kg m^{-3} and 77.1 mPa·s, respectively. The acid, saponification, and iodine values of the oil, determined according to the AOCS official methods, were 0.29 mg KOH/g, 190 mg KOH/g, and 139 g I$_2$/100 g, respectively [48]. The oil consisted of the following fatty acids: palmitic acid (7.3 %), stearic acid (4 %), oleic acid (26 %), and linoleic acid (62.2 %) [49].

Certified methanol of 99.5 % purity was from Zorka Pharma (Šabac, Serbia). Methanol, 2-propanol, and *n*-hexane, all HPLC grade, were obtained from LAB-SCAN (Dublin, Ireland).

2. 2. Catalyst preparation

Wheat straw was completely combusted in a shallow metal tray at open air. Cold ash, called fresh WSA (fWSA) was collected, crushed using a porcelain mortar and pestle, sieved through a 1 mm sieve, and placed in a glass bottle, which was then stored in a desiccator. The WSA stored for 40 days, called the aged WSA (aWSA), did not show any activity in the methanolysis reaction of sunflower oil even after thermal activation at 150 °C. The fWSA catalyst was separated from the reaction mixture after completing the reaction by decanting, washed twice with 20 ml of methanol and then with 20 ml of *n*-hexane, dried in an oven at 120 °C for 15 min, and then cooled down in a desiccator. The separated

catalyst eventually used in the subsequent reactions is called spent WSA (sWSA after the first use; sWSA1, sWSA2, and sWSA3 after the first, second, and third reuse, respectively).

2. 3. Catalyst characterization

The X-ray powder diffraction measurements were performed by a Rigaku Smartlab diffractometer (Rigaku, Japan) equipped with a D/teX Ultra 250 strip detector using $CuK_{\alpha1,2}$ (*U* = 40 kV and *I* = 30 mA) with low-background single-crystal silicon sample holders. The measurement was conducted in the 2θ = 10-70° domain, step-length of 0.01° and the rate of 5° / min.

Characterization of the fWSA, aWSA, sWSA, and sWSA3 samples by temperature-programmed decomposition (TPDe) was performed in the temperature range 50-800 °C with 60 min dwell time at the maximum temperature and the helium flow (20 cm^3 min^{-1}), using a TPDRO 1100 device (Thermo Scientific, Italy). In addition to the thermal conductivity detector (TCD), the device was also equipped with a ThermoStar GSD320 mass detector (Pfeiffer Vacuum, Germany). Prior to the measurement, each sample was dried in an oven at 110 °C for 24 h, transferred to a quartz tubular reactor at 40 °C, where it was held in the helium stream (20 cm^3 min^{-1}) for 60 min to eliminate possible adsorbed H_2O. Thereafter, CO_2 was adsorbed on the sample from a gas mixture of 16.2 % CO_2/He at the temperature of 40 °C and a flow rate of 20 cm^3 min^{-1} for 60 min. Finally, after cleaning the system and reactor lines of residual CO_2 with pure helium (20 cm^3 min^{-1} for 60 min), the sample was heated in a helium stream as described.

To determine morphology characteristics and chemical composition of fWSA, aWSA, sWSA, and sWSA3, they were analyzed by a scanning electron microscope (SEM) JEOL JSM-6610LV (Jeol, Japan) equipped with a secondary electron (SE) detector and energy-dispersive spectrometer (EDS) (Oxford Instruments, UK). Before the measurement, the samples were prepared by deposition of thin gold vapor layer on the catalyst surface employing the cool sputter coater LEICA SCD005 (Leica Microsystems, Germany).

Textural properties of fWSA and aWSA samples were determined by N_2 physisorption at -196 °C and mercury porosimetry. The adsorption-desorption isotherms were obtained by N_2 physisorption measurements at -196 °C by using a Sorptomatic 1990 device (Thermo Finnigan, Italy). The sample preparation procedure included drying in an oven for 4 h, transfer of the samples into a measuring burette and drying in a vacuum in regime 4 h at 110 °C and 18 h at 250 °C. The specific surface areas (SSA_{BET}) of the samples were calculated from the linear part of the adsorption isotherm by applying the Brunauer-Emmett-Teller (BET) equation [50]. The Dubinin-Radushkevich method [51] was used to determine the micropore volume (V_{mic}) while the mesopore volume (V_{mes}) was estimated by the Barrett, Joyner, and Halenda (BJH) method [52] from the desorption branch using the Lecloux standard isotherm [53].

Before the mercury porosimetry measurement, a sample was dried in an oven at 110 °C for 24 h, cooled in a desiccator and then placed in a sample holder and vacuumed for 2 h at room temperature. The bulk density was determined by a Macropore Unit 120 (Fisons Instruments, Italy), and after that, in the pressure range of 0.1-200 MPa Hg, the mercury porosimetry was conducted in a high-pressure unit PASCAL 440 (Thermo Fisher, Italy). In a high-pressure unit, for each sample, two consecutive intrusion-extrusion measurements (Run 1 and Run 2) were performed to determine the contribution of the interparticle and intraparticle space (*i.e.*, voids and pores, respectively) of the material porosity. A SOLID Software System PC interface was used for automatic data acquisition and all textural parameter calculations.

2. 4. Methanolysis reaction

The batch methanolysis reaction was carried out in a three-neck round-bottomed flask (250 cm^3) equipped with an upright reflux condenser and a magnetic stirrer. The reaction flask was placed in a water bath and kept at the desired temperature. Measured amounts of the fWSA catalyst and methanol were added to the reaction flask and maintained at the desired temperature for 15 min. The predetermined quantity of sunflower oil was heated at the same desired temperature and then poured into the reaction flask. As soon as the sunflower oil was added, agitation (900 rpm) and time measuring started. During the reaction, samples (1 cm^3) of the reaction mixture were withdrawn (at specified time intervals), poured into Eppendorf tubes, and immediately placed in ice-cold water to terminate the reaction. The

samples were then centrifuged (3500 rpm for 15 min). The fatty acid methyl esters (FAME)-oil layer was separated, dissolved in a solution of a mixture of 2-propanol and *n*-hexane (5/4 v/v) in a ratio 1/200, filtered through a Millipore filter (0.45 μm), and analyzed by the High Performance Liquid Chromatography (HPLC) method described elsewhere [54]. The methanolysis reaction was tested at the temperatures of 55, 60, and 65 °C, the catalyst loading of 10, 15 and 20 % of the oil weight and the methanol-to-oil molar ratio 18:1, 21:1, and 24:1. Kostić *et al.* [20] observed that an increase of the reaction temperatures from 45 to 65 °C accelerated the reaction significantly and shortened its duration from 7 h to 4 h. In a preliminary experiment conducted at 60 °C, using the catalyst amount of 10 % (based on the oil weight) and the methanol-to-oil molar ratio of 18:1, the reaction was completed after about 4 h. Therefore, the temperature of 55 °C was selected as the lower limit. The temperature of 65 °C was taken as the maximally possible upper value as the boiling point of methanol is 64.7 °C. In addition, the preliminary experiments showed that a larger quantity of methanol was required to distribute very voluminous WSA uniformly in the reaction mixture. Consequently, higher methanol-to-oil molar ratios were employed.

Leaching of catalytically active species was examined using the same procedure carried out under the optimal reaction conditions. The appropriate amounts of methanol and fWSA were stirred magnetically for 124 min under the optimized reaction conditions following the above-described procedure. After being separated from the catalyst, methanol was used in the reaction with sunflower oil without the presence of the catalyst, as described above. The preliminary thin layer chromatography (TLC) analysis of the centrifuged samples of the reaction mixture showed that FAME was not formed, indicating no leaching of the active species.

2. 5. Statistical modeling and optimization

FAME content was correlated with four process factors, namely the reaction temperature, *A* (55, 60, and 65 °C), the catalyst loading, *B* (10, 15, and 20 % of the oil weight), the methanol-to-oil molar ratio, *C* (18 : 1, 21 : 1, and 24 : 1), and the reaction times, *D* (60, 120, 180, and 240 min), combining the RSM and a historical data design (total 70 runs). The experimental matrix of the historical data design is presented in Table S-1 (Supplementary Material). The data were normally distributed, and outlier value was not present (Fig. S-1, Supplementary Material). The experiments were conducted in random order. The following quadratic equation was used:

$$Y = b_0 + b_1A + b_2B + b_3C + b_4D + b_{12}AB + b_{13}AC + b_{14}AD + b_{23}BC + b_{24}BD + b_{34}CD + b_{11}A^2 + b_{22}B^2 + b_{33}C^2 + b_{44}D^2 \qquad (1)$$

where Y is the FAME content, *A*, *B*, *C* and *D* are process factors, b_0 is the constant regression coefficient, b_i are linear regression coefficients (i = 1, 2, 3, 4), b_{ij} are two-factor interaction regression coefficients (i = 1, 2, 3; j = i +1), and b_{ii} are quadratic regression coefficients (i = 1, 2, 3, 4). The parameters of the quadratic equation were calculated by the non-linear regression method using the Design Expert software (StatEase, USA). Statistical significance of the process factors and their interactions was estimated with a confidence level of 95 % by the analysis of variance (ANOVA). The developed model was statistically assessed by the coefficient of determination, R^2, the predicted coefficient of determination, R^2_{pred}, the adjusted coefficient of determination, R^2_{adj}, the F_{model}- and *p*-values, the adequate precision *Adeq. Prec.*, the coefficient of variation, *C.V.*, the mean relative percent deviation *MRPD*, and the lack of fit F_{LOF}. The developed model was then modified by eliminating statistically insignificant terms. Several optimization points, which provided the maximum actual FAME content for a set of reaction conditions, were also determined by the Design Expert software.

3. RESULTS AND DISCUSSION

3. 1. Catalyst characterization

3. 1. 1. Elemental composition of the fWSA catalyst

The average elementary composition of the fWSA sample, based on three EDS spectra for three different positions is presented in Table 2. Although the content of Si, C, and O represents amounts 86 and 90 % of the total detected elements, differences in the contents of Si and C, determined at individual sites, indicate some inhomogeneity of the fWSA sample, most likely due to differences in the presence of some form of silicate phase.

Table 2. Elemental composition of the fWSA catalyst

Spectrum	Content, wt.%								
	C	O	Na	Mg	Si	Cl	K	Ca	Total
1	50.0	23.3	BDL	1.3	12.6	1.4	9.0	2.4	100
2	51.2	21.0	BDL	1.4	17.4	1.2	6.3	1.6	100
3	23.1	42.4	BDL	0.5	24.5	1.4	7.7	0.5	100
Average ± STD	41.4±15.9	28.9±11.8	BDL	1.1±0.5	18.2±6.0	1.3±0.1	7.7±1.4	1.5±0.9	100

*BDL – below detection limit

Dodson [42] pointed out that the physico-chemical properties and elemental composition of WSA depended on the initial elements in wheat straw, which further depend on the wheat straw variety, growing conditions, and biomass species. Similar dependence of the walnut shells elemental composition on geographical region and cultivation conditions was reported by Vassilev [55]. In another study [22] it was found that various potassium (KCl, K_2CO_3), and calcium ($CaMgSiO_4$, $Ca_3(PO_4)_2$) compounds were responsible for the catalytic activity of tucuma peel ash.

3. 1. 2. XRD characterization of the WSA catalysts

X-Ray Diffraction (XRD) patterns of the fWSA, aWSA, sWSA, and sWSA3 (after the third reuse) samples are shown in Figure 1.
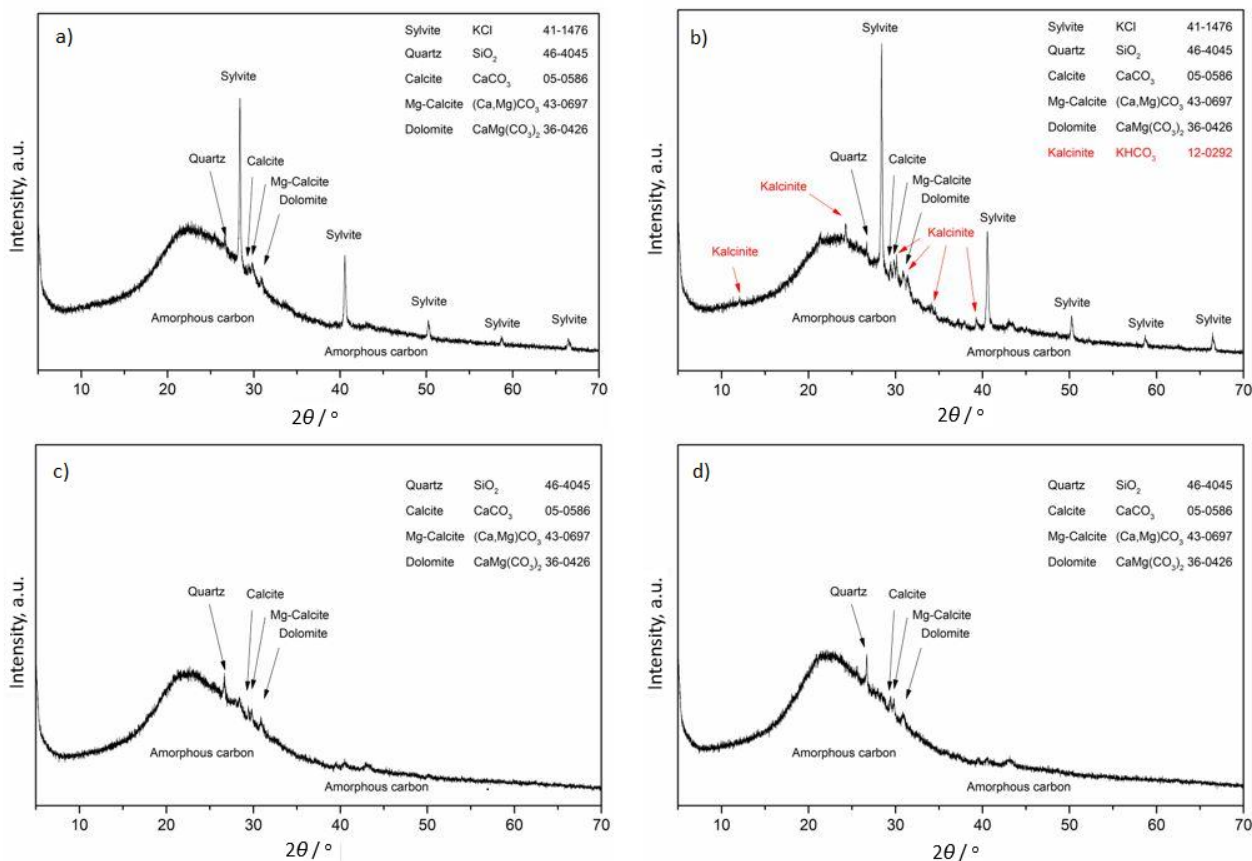

Figure 1. XRD patterns of (a) fWSA (b) aWSA, (c) sWSA (after the first use), and (d) sWSA3 (after the third reuse)

The broad peak (hump) at 23° 2θ is characteristic for any residue of incomplete combustion of biological materials, *i.e.*, biochar, indicating its dominantly amorphous carbon structure [56]. Still, the color of fWSA and aWSA samples was black, suggesting that a significant part of the obtained materials was carbon.

The XRD pattern of the fWSA sample confirms the presence of five phases:
1) quartz (SiO_2) with a characteristic peak at 2θ = 26.64° (PDF#46-1045);
2) calcite ($CaCO_3$) with a characteristic peak at 2θ = 29.41° (PDF#05-0586),

3) dolomite $CaMg(CO_3)_2$ with a characteristic peak at $2\theta = 30.94^o$ (PDF#36-0426),

4) Mg-calcite $(Ca,Mg)CO_3$ with a characteristic peak at $2\theta = 29.71^o$ (PDF#43-0697), and

5) sylvite (KCl) with characteristic peaks at $2\theta = 28.35, 40.51, 50.17, 58.64,$ and 66.38^o (PDF#41-1476).

This mineralogical composition is not unusual for biochars. Moreover, calcite, Mg, Ca-carbonate ($Ca_xMg_{(1-x)}CO_3$), and quartz were the most common crystalline phases identified in biochars [56,57]. In the literature, the presence of quartz in biochar is always associated with contamination of the raw materials from the soil (even after thorough washing) while the presence of the carbonate phases, in addition to the mentioned explanation, is related to the presence of carbonates in the original biomass, and even formation by the entrapment of CO_2, evolving from the thermal decomposition of organic carbon, in the alkaline charred material [56].

Except for sylvite (KCl), the diffractograms of the sWSA and sWSA3 samples (Fig. 1c, d) show the presence of reflections corresponding to the same phases identified in the fWSA sample. In fact, even the strongest reflection of sylvite at 28.4° 2θ is hardly noticeable on the diffraction sample of the sWSA sample and is almost non-existent for the sWSA3 sample (Fig. 1d). Therefore, the observed differences in activity between the fWSA, sWSA, and sWSA3 samples are directly related to the sylvite phase (*i.e.*, K^+ ions) content in the materials.

An uncommon result was obtained for the aWSA sample. A new phase of $KHCO_3$ appeared in the diffractogram (peaks at 12.05, 31.22, 34.06, 39.20°, with the dominant peak at $2\theta = 24.23^o$), which was not detected for the fWSA sample. As $KHCO_3$ is barely soluble in methanol [58], it forms a protective layer on the surface of KCl particles, so that almost all KCl or K^+ ions are inaccessible (blocked) for the reaction.

It is worth noting that the applied process of burning wheat straw did not create the conditions for obtaining CaO by decomposing calcite, Mg-rich calcite, and/or Ca-rich dolomite in the fWSA sample. This suggests that the achieved combustion temperature was not sufficiently high to decompose the carbonate phases, forming CaO and CO_2. Even, at a sufficiently high temperature to decompose the carbonates, CO_2 was formed, changing the atmosphere, which shifted the reaction to the carbonate formation; in other words, the carbonate decomposition was prevented.

3. 1. 3. TPDe of fWSA and aWSA samples

TPDe profiles after CO_2 adsorption by the fWSA and aWSA samples, shown in Figure 2, confirm incomplete carbonization of wheat straw in the applied combustion procedure, as suggested by the results of XRD measurements. Thermal conductivity detector (TCD) signals of both materials did not reach the baseline value in the entire temperature range, even at the highest temperature of 800 °C.
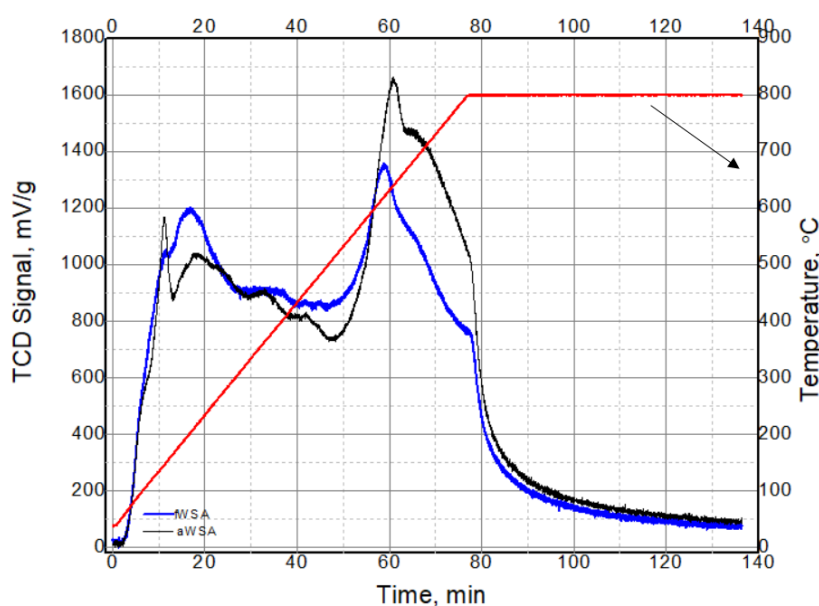

Figure 2. TCD signals of aWSA and fWSA samples

However, difference in the areas below the curves for the freshly carbonized sample (fWSA) and the sample left for 40 days (aWSA) is evident, in favor of the aWSA. The finding is somewhat strange as it is expected that the CO_2 adsorption capacity will be either the same for both materials or larger in the case of a freshly prepared catalyst (fWSA sample). The experimental setup can be ruled out as the cause of the observed difference because the profile of a sample aged for 150 days (aWSA-150) is practically identical to the profile of the 40-day-old sample (aWSA), as can be seen in Figure S-2 (Supplementary Material).

The unexpected results shown in Figure 2 could be most likely related to the composition of the gas phase during temperature-programmed heating the samples. If the sample decomposed during heating, other gaseous components (*e.g.*, CO, H_2O, and even a fraction of organic molecules) could be found in the carrier gas stream (helium), beside the desorbed CO_2. As the TC detector was not selective, the obtained profile would represent a function of the content and thermal conductivity of all gases formed during the TPD measurement. Better insight can be obtained by analyzing the output mixture of gases using mass spectroscopy (MS). The experimental setup was performed in such a way that the sampling for MS measurements takes place at the position before the trap (Mg-perchlorate) that removes H_2O and the obtained results are shown in Figure 3.
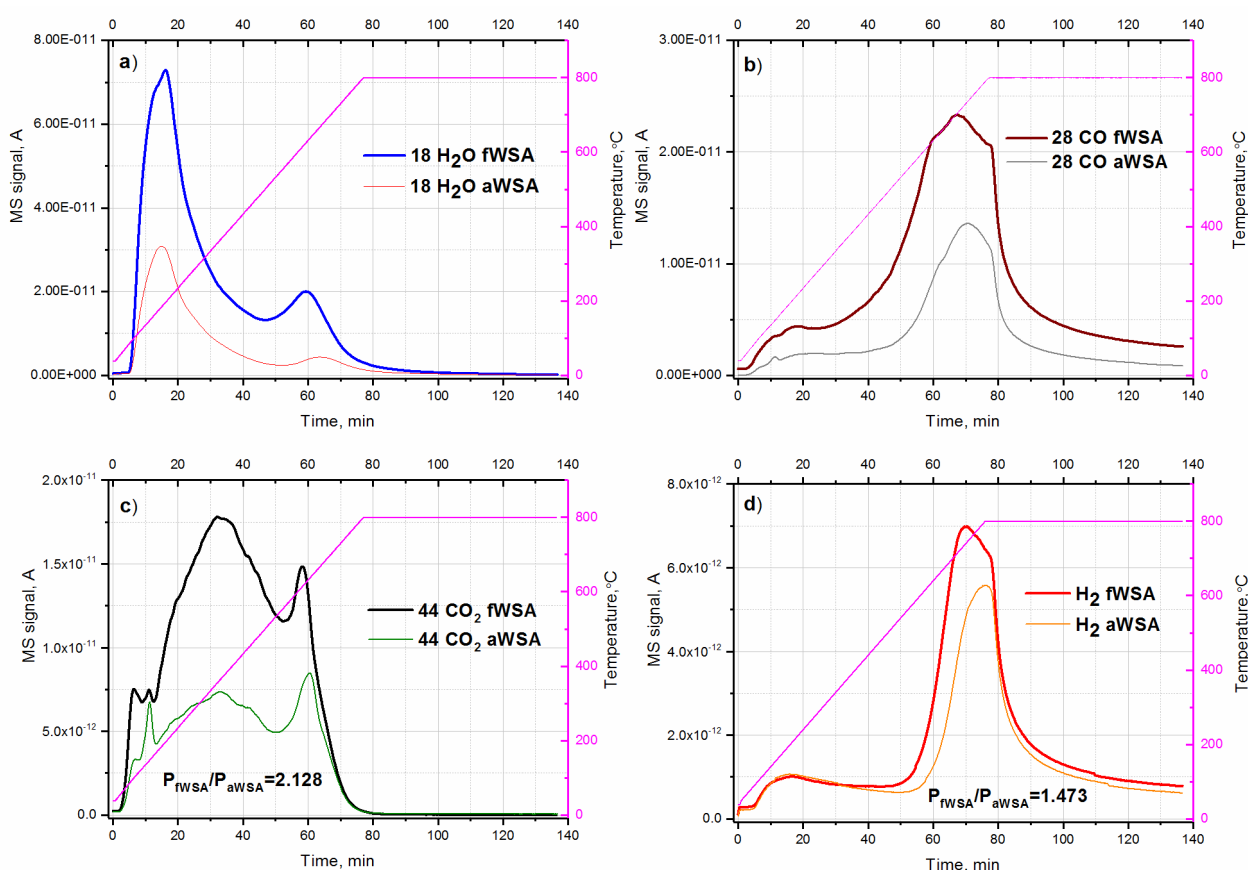

Figure 3. MS signals of H_2O (a), CO (b), CO_2 (c), and H_2 (d) for fWSA and aWSA samples

All selected MS signals (H_2, H_2O, CO, and CO_2) were more intensive for the fWSA sample than for the aWSA sample (Fig. 3), which was not in accordance with the results of TCD in the temperature range of 500-800 °C (Fig. 2). H_2O, CO, and CO_2 have thermal conductivities remarkably lower than the carrier gas. So, the presence of these gases in the carrier gas would reduce the thermal conductivity of the gas mixture, which was detected as an increase in the TCD signal. Since Mg-perchlorate is set as an H_2O trap before the TCD measurement line, the contribution of H_2O in the registered TCD signal is not present. However, in that case, the TCD signal of the fWSA sample would have been higher than the TCD signal of the aWSA sample in the whole applied temperature range (including the range of 500-800 °C). This leads to the conclusion that there must be some other components present in the gas, which decreased the TCD signal of the

fWSA sample. The only remaining gas was H_2. The hydrogen signal registered by the MS detector for the fWSA sample was about 47 % higher (Fig. 3d) than that for the aWSA sample. As the thermal conductivity of hydrogen is higher than the thermal conductivity of the carrier gas which passes through the reference branch of the TC detector, the presence of H_2 in the gas mixture leaving the reactor and passing through the measuring branch of the TC detector causes a decrease in the registered signal. Overall, the hydrogen contribution (signal decrease) exceeds the contribution of CO and CO_2 (signal increase), so the registered TCD signal of the fWSA sample is weaker than that registered for the aWSA sample.

It is worth mentioning that the area below the MS-CO_2 profile for the fWSA sample is more than twice higher than that of the aWSA sample (Fig. 3c). Except for the aging time, the two samples were treated equally, so the different amounts of CO_2 released by sample decomposition could be hardly expected. As the masses of the two samples used for the analysis were almost the same (the difference of less than 2 %), it was clear that the difference in the MS-CO_2 signals was due to different amounts of CO_2 desorbed from the fWSA and aWSA samples. As the desorbed amount of CO_2 is unambiguously connected to the alkalinity of the catalyst surface, the activity of the freshly prepared catalyst has to be higher than that of the aged catalyst.

3. 1. 4. Textural properties of the fWSA and aWSA catalysts

Textural parameters of the fWSA and aWSA samples obtained by low-temperature N_2 physisorption at 77 K and Hg porosimetry measurements are given in Table 3.

Table 3. Textural parameters of the fWSA and aWSA samples obtained by Hg porosimetry and low-temperature N_2 physisorption at 77 K

Method		Hg porosimetry[a]					N_2 physisorption at 77 K[b]		
Sample		V_{tot-Hg} / cm^3 g^{-1}	ρ_{app} / g cm^{-3}	ρ_{bulk} / g cm^{-3}	SSA_{Hg} / m^2 g^{-1}	Porosity, %	V_{mes} / cm^3 g^{-1}	V_{mic} / cm^3 g^{-1}	SSA_{BET} / m^2 g^{-1}
fWSA	Run 1	1.114	0.89	0.45	11.5	49.8	0.041	0.039	98.5
	Run 2	0.095	0.89	0.82	3.1	7.8			
aWSA	Run 1	1.420	1.11	0.43	12.9	61.1	0.029	0.038	90.7
	Run 2	0.066	1.11	1.03	2.9	6.8			

[a]V_{tot-Hg} – the total cumulative volume, ρ_{app} – the apparent density, ρ_{bulk} – the bulk density, SSA_{Hg} – the total specific surface area;
[b]V_{mes} – mesopores volume, V_{mic} – the micropore volume, SSA_{BET} – the specific surface area.
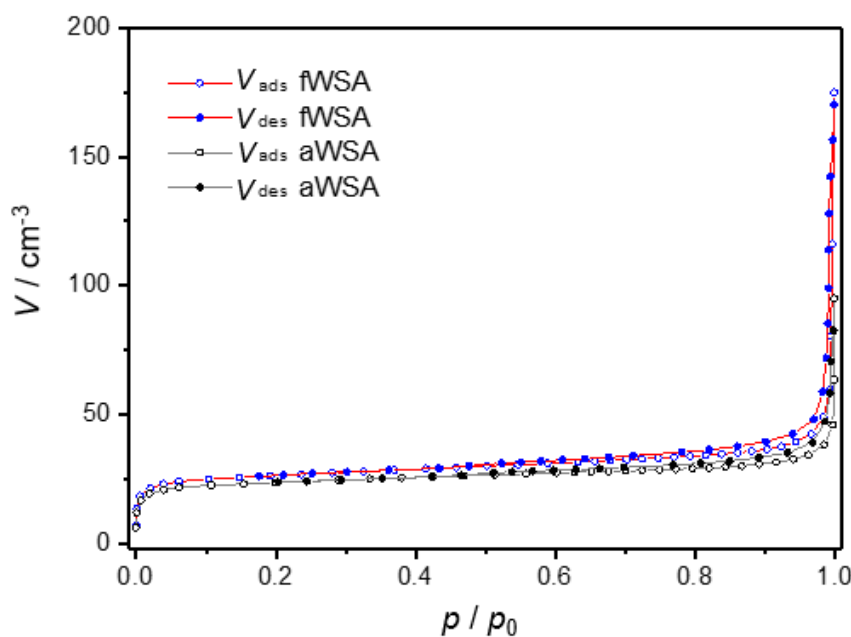

Fig. 4 N_2 adsorption-desorption isotherms of the fWSA and aWSA catalysts

The N_2 adsorption-desorption isotherms of the materials (Fig. 4) are similar and belong to the type II, which is associated with nonporous and macroporous materials. For both materials, the microporous volume is similar (0.040 $cm^3\,g^{-1}$) while the mesoporous volume (V_{mes}) values of the fWSA are for 40 % higher than those of the aWSA, but both values are small. Additionally, the obtained values of the total specific surface area, SSA_{BET}, are considerable and slightly higher for the fWSA compared to that for aWSA (98.5 $m^2\,g^{-1}$ *vs.* 90.7 $m^2\,g^{-1}$).

Further information on the textual properties of both materials can be obtained by analyzing the results of Hg porosimetry measurements (Table 3. and Fig. 5). Due to the small volume of intruded Hg and the clearer presentation of the results, the extrusion-intrusion curves of the Run 2 for the fWSA and aWSA samples are omitted from Fig. 5.
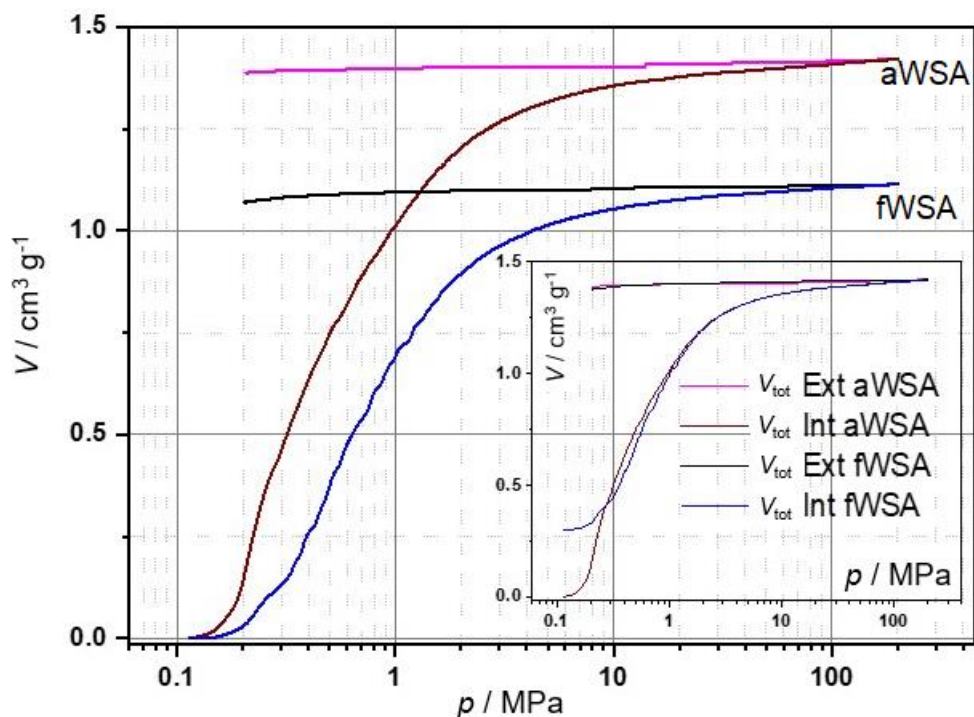

Figure 5. Intrusion/extrusion curves of Hg obtained in Run 1 for the fWSA and aWSA samples; insert: the shifted intrusion/extrusion curves of Run 1 of the fWSA sample

For both materials, the total cumulative volume ($V_{tot\text{-}Hg}$) in Run 1 is quite high, significantly above 1 $cm^3\,g^{-1}$. The $V_{tot\text{-}Hg}$ value of the aWSA sample is higher than that of the fWSA sample, pointing out to different initial interparticle fillings of these materials. In other words, the fWSA sample settles better in the dilatometer than the aWSA sample. The difference in $V_{tot\text{-}Hg}$ can be detected at the intrusion pressures lower than 270 kPa, which corresponds to the pore diameter (D_p) domain from 14 to 5.5 µm. For the intrusion pressures higher than 1 MPa ($D_p <$ 1.5 µm), difference in the $V_{tot\text{-}Hg}$ and Hg intrusion location was not observed (insert in Fig. 5). Additionally, the Run 1 extrusion curves (Fig. 5) for both samples were nearly horizontal, indicating that almost the whole mercury-filled space for both samples were the interparticle space since Hg was not released during the pressure decrease.

It is worth noting that the SSA_{BET} values obtained from the N_2 physisorption measurements are considerably higher than SSA_{Hg} values obtained by the Hg porosimetry measurements (independent of the measurement cycle). Obviously, the most significant part of the specific surface area of the carbonized material originates from the outer surface of the material particles and/or the pore type (micropores and mesopores less than 7.5 nm) inaccessible to the Hg porosimetry measurement.

The huge reduction in the $V_{tot\text{-}Hg}$ value for Run 2, compared to the $V_{tot\text{-}Hg}$ value for Run 1 for both samples clearly show that during the Hg intrusion process of Run 1 compacting of the powder occurred, which is the main reason for differences in porosity obtain for the Runs 1 and 2 (Table 3). Finally, extremely low porosity obtained for the fWSA (7.8 %) and aWSA (6.8 %) samples from $V_{tot\text{-}Hg}$ Run 2, classify these materials as nonporous (for the measured pore diameter range).

Figure 6 shows micrographs of fWSA and sWSA3 samples at different magnifications. At the lowest magnification, there is a clear difference between particle dimensions of the fWSA and WSA3 samples. The particle dimensions of fWSA are larger compared to sWSA3, which can be attributed to the comminution of sWSA3 particles during the catalytic tests caused by mechanical stirring and collision of the catalyst particles. The difference between these two micrographs demonstrates shredding intensity. An even better representation of the difference in the catalyst particle dimensions between fWSA and sWSA3 is seen at the higher magnification (Fig. 6, middle row, magnifications 250×).
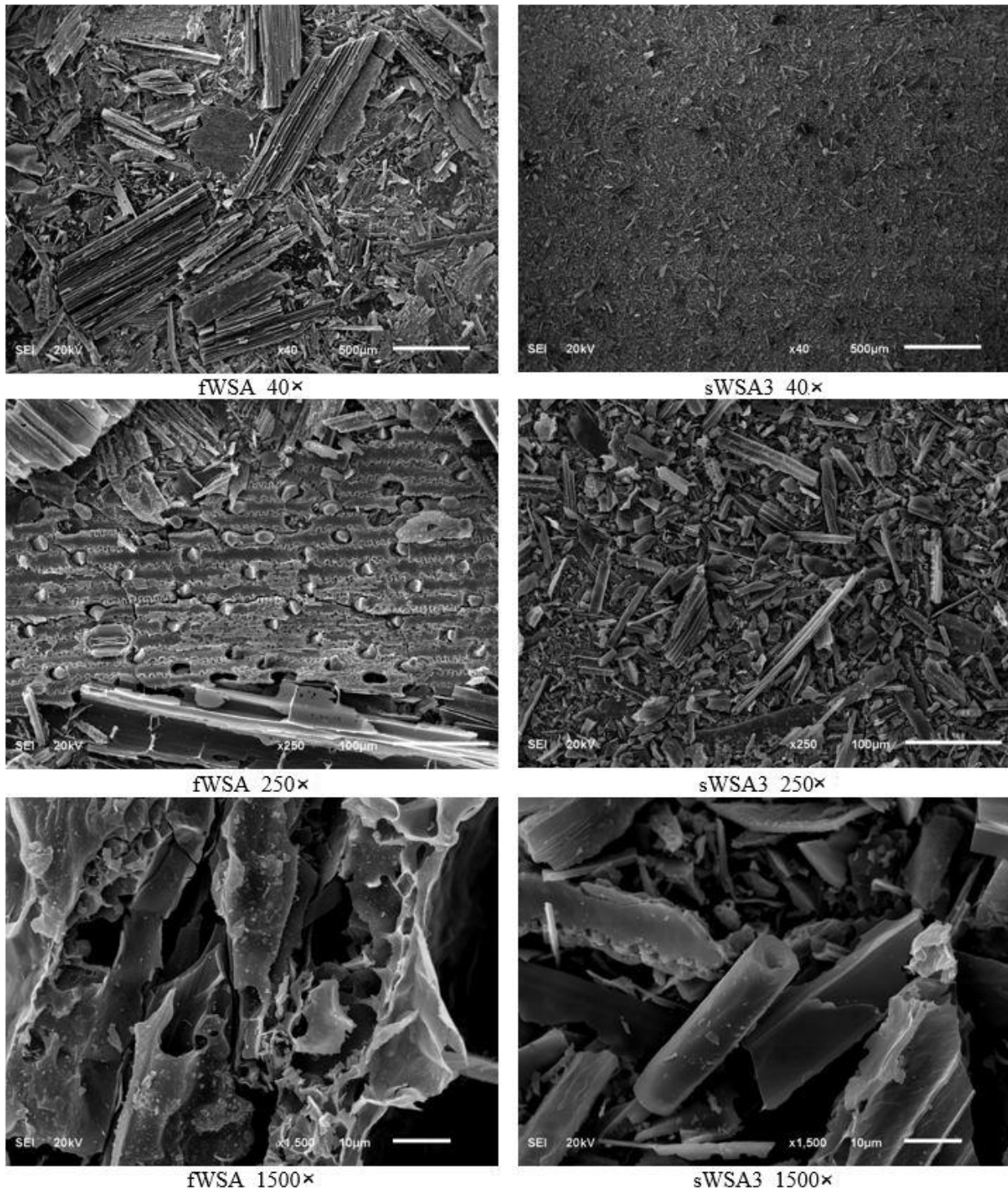

Fig. 6 Micrographs of fWSA (left column) and sWSA3 (right column) samples at different magnifications (scale bars: the top row = 500 μm; the middle row = 100 μm; the bottom row = 10 μm)

3. 2. Catalytic testing of the fWSA catalyst

Figure 7 demonstrates the catalytic activity of the fWSA catalyst in methanolysis of sunflower oil by showing sigmoid variations of FAMEs and triacylglycerols (TAGs) contents with time. At the reaction temperature of 55 °C, the catalyst loading of 15 %, and the methanol-to-oil molar ratio of 18:1, the FAME content increases on account of a decrease in the TAG content with the progress of the reaction while low contents of intermediates, monoacylglycerols (MAGs) and diacylglycerols (DAGs), slightly increase with time, reaching the maxima (about 0.1 % MAGs and 1.0 % DAGs) and then remain nearly constant or decrease slightly until the reaction is completed. These variations are typical for methanolysis reactions of vegetable oils.
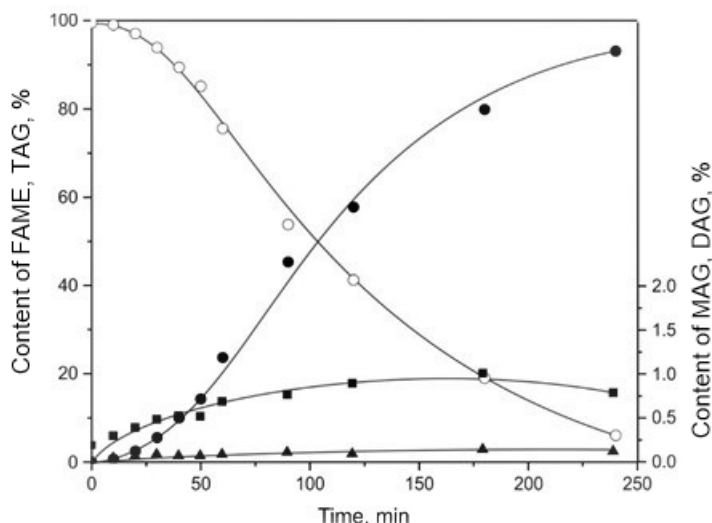

Figure 7. Variation of the reaction mixture composition with the progress of sunflower oil methanolysis catalyzed by fWSA (the reaction temperature of 55 °C, the catalyst loading of 15% of the oil weight, and the methanol-to-oil molar ratio of 18:1; FAMEcontent - ●, MAG content - ▲, DAG content - ■, and TAG content - ○)

A CaO–based palm kernel ash showed similar catalytic activity as the fWSA catalyst, giving the yield of 99 % in 240 min [20]. The catalytic activity of most agro-waste-based ashes presented in Table 1 is based on K-species, showing similarly high yields but in shorter reaction times, which indicates higher activity than that of the fWSA catalyst.

Physicochemical properties of the biodiesel obtained from sunflower oil using methanol and the fWSA catalyst under the optimal reaction conditions (the reaction temperature of 60.3 °C, the catalyst loading of 11.6 % of the oil weight, the methanol-to-oil molar ratio of 18.3:1, and the reaction time of 124 min) are compared in Table 4 with the limit values prescribed by the EN 14214 biodiesel quality standard. The contents of FAMEs (98.6 %) and MAGs (0.2 %) in the obtained biodiesel product were within the standard limits (>96.5 and <0.7 %, respectively) while the contents of DAGs (0.8 %) and TAGs (0.3 %) were higher than the specified limits (<0.2 %), requiring further purification of the obtained biodiesel. Depending on the concentration of unreacted TAG and DAG in biodiesel, its viscosity can increase, causing a reduction in the combustion efficiency, clogging of the fuel filter, and deposition on engine parts such as pistons, valves, and injector nozzles [59].

Table 4. Physiochemical properties of the biodiesel obtained over the fWSA catalyst

Property	FAME	EN 14214
Density (15 °C), kg m^{-3}	866.9	860-900
Kinematic viscosity (40 °C), m^2 s^{-1}	3.69×10^{-6}	(3.5-5.0) ×10^{-6}
Acid value, mg KOH g^{-1}	0.1	0.50 max
Iodine value, g I$_2$ (100 g)$^{-1}$	110	120 max
Water content, mg kg^{-1}	490	500 max
FAME content, %	98.6	96.5 min
MAG content, %	0.2	0.7 max
DAG content, %	0.8	0.2 max
TAG content, %	0.3	0.2 max

Decrease in the catalytic activity with the repeated use of the spent catalyst is shown in Figure 8. The WSA-based catalyst loses the catalytic activity in each subsequent use under the optimal reaction conditions determined by the statistical optimization, which is undesirable. After the first and second reuse, the FAME content after the reaction time of 4 h decreased to 37 and 12 %, respectively, while it was only 3 % after the third reuse. The decrease in the FAME content with the catalyst reuse could be due to the incomplete separation of the fWSA catalyst from the reaction mixture, partial deactivation of the catalyst during the reaction and separation or covering the surface of the catalyst by the reaction products that reduces the number of active sites.
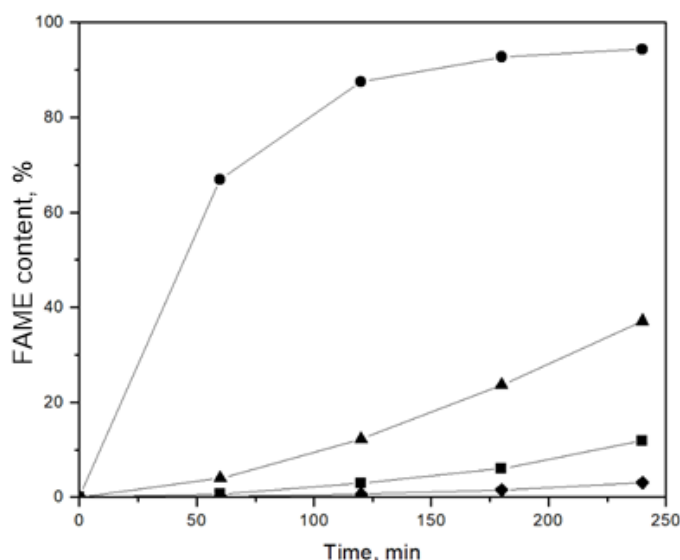

Figure 8. FAME content as a function of reaction time in the repeated use of the WSA catalyst: fWSA - •; sWSA1 (first reuse) - ▲; sWSA2 (second reuse) - ■; and sWAS3 (third reuse) - ♦ (optimal reaction conditions: the reaction temperature of 60.3 °C, the catalyst loading of 11.6 % of the oil weight, and the methanol-to-oil molar ratio of 18.3:1)

3. 3. Analysis of the methanolysis reaction

Generally, transesterification of TAG is affected by four main operating conditions: reaction temperature, methanol-to-oil molar ratio, catalyst loading, and reaction time, as can be seen in Figure 9.
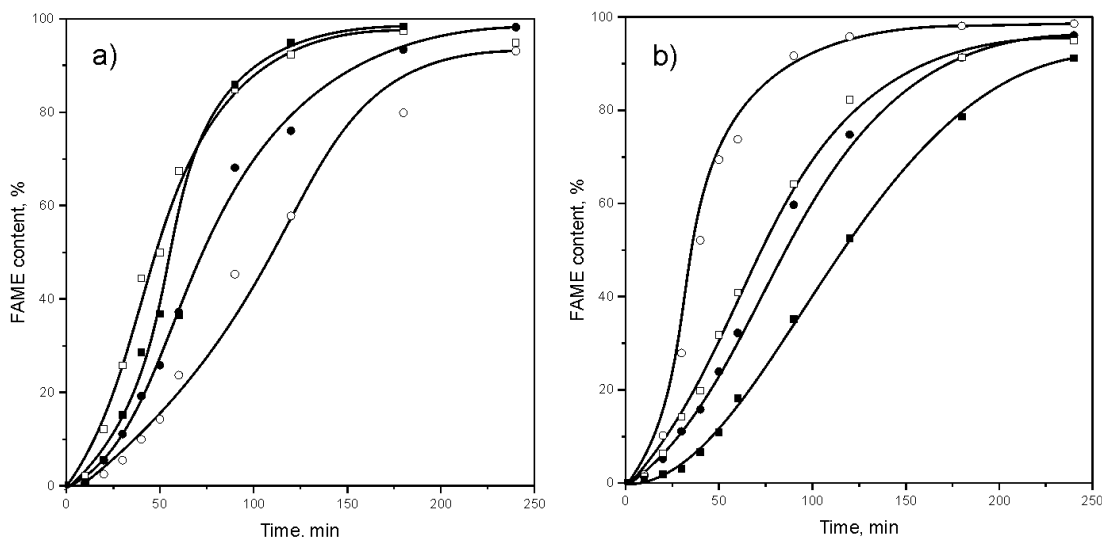

Figure 9. FAME content as a function of the reaction time at different reaction conditions. a) Influence of the reaction temperature and methanol-to-oil molar ratio on FAME synthesis at the catalyst loading of 15 % (reaction temperature 55 °C: methanol-to-oil molar ratio: 18:1 – ○, 24:1 – ● and reaction temperature 65 °C: methanol-to-oil molar ratio: 18:1 – □, 24:1 – ■; b) Influence of the catalyst loading and methanol-to-oil molar ratio on FAME synthesis at the reaction temperature of 60 °C (methanol-to-oil molar ratio: 18:1: catalyst loading: 10 % – ○, 20 %– ● and methanol-to-oil molar ratio: 24:1: catalyst loading: 10 % – □, 20 % – ■)

Figure 9a shows the FAME content at the catalyst loading of 15 %, two different reaction temperatures (55 and 65 °C) and two methanol-to-oil molar ratios (18 : 1 and 24 : 1). At the lower methanol-to-oil molar ratio (18 : 1), the reaction rate increased with the temperature rise. The importance of the reaction temperature came out from the increase in the reaction rate constant at higher temperatures, which accelerated the FAME synthesis. However, the reaction temperature showed negligible influence on the FAME synthesis at the higher methanol-to-oil molar ratio (24 : 1), thus implying that its influence in the applied range (55-65 °C) was repressed by the increased methanol-to-oil molar ratio.

The FAME content variations with time at a constant reaction temperature (60 °C) at different catalyst loadings (10 and 20 %) and methanol-to-oil molar ratios (18 : 1 and 24 : 1) are compared in Figure 9b. As can be seen, the reaction rate decreased with increasing the catalyst loading for both methanol-to-oil molar ratio. The reaction rate at 10 % of catalyst loading was higher for the lower methanol-to-oil molar ratio while the slowest reaction was observed at the catalyst loading of 20 % and the methanol-to-oil molar ratio of 24:1. This could be explained by aggravated mixing and poor contact of the liquid phase with the active sites of the catalyst.

3. 4. Statistical modeling and optimization

Acceptability of the statistical models was firstly tested by the sequential sum of squares, lack of fit, and model summary statistic tests that aimed at selecting the model having the highest order, insignificant lack-of-fit and maximized the R^2_{adj} and R^2_{pred} values, respectively. According to these tests, the aliased cubic model was disregarded while the quadratic model was suggested as it had the highest order and the highest R^2, R^2_{adj}, and R^2_{pred} values among the other models (Tables S-2 and S-3, Supplementary Material) despite its significant lack-of-fit (Table S-4, Supplementary Material). Hence, the quadratic model was further evaluated by the ANOVA (Table 5) that confirmed its significance by its high *F*-value (20.99) and its low *p*-value (< 0.0001). The quadratic equations in terms of coded and actual process factors are given in the Supplementary material, Eqs. (S-1) and (S-2)**.** The ANOVA showed that at a confidence level of 95 % only the catalyst loading (*B*), the reaction time (*D*), and their interaction (*B*x*D*), as well as the squared reaction temperature, catalyst loading, and reaction time (A^2, B^2, and D^2) were significant model terms (Table 5).

Table 5. ANOVA results for the quadratic model

Source	Sum of squares	Degree of freedom	Mean square	*F*-value	*p*-value
Model	38212.0	14	2729.4	20.99	**< 0.0001**
A	111.5	1	111.5	0.86	0.358
B	5198.9	1	5198.9	39.99	**< 0.0001**
C	229.2	1	229.2	1.76	0.190
D	21110.2	1	21110.2	162.37	**< 0.0001**
*A*x*B*	98.1	1	98.1	0.75	0.389
*A*x*C*	486.1	1	486.1	3.74	0.058
*A*x*D*	189.3	1	189.3	1.46	0.233
*B*x*C*	1.7	1	1.7	0.01	0.908
*B*x*D*	1101.7	1	1101.7	8.47	**0.005**
*C*x*D*	227.2	1	227.2	1.75	0.192
A^2	2733.2	1	2733.2	21.02	**< 0.0001**
B^2	4258.9	1	4258.9	32.76	**< 0.0001**
C^2	108.2	1	108.2	0.83	0.366
D^2	2813.4	1	2813.4	21.64	**< 0.0001**
Residual	7150.8	55	130.0		
Lack of Fit	7115.4	50	142.3	20.10	**0.002**
Pure Error	35.4	5	7.1		
Corrected Total	45362.7	69			

Having the highest *F*-value of 162.37, the reaction time was the most important variable affecting the FAME content, followed by catalyst loading, which agreed with the optimization results of the methanolysis of corn germ oil using corn cobs ash as a catalyst [27]**.** On the other hand, Kostić *et al.* [20] showed for methanolysis of sunflower oil over palm kernel shell biochar that the reaction temperature and the methanol-to-oil molar ratio were statistically significant for the FAME content while the effect of catalyst loading was statistically insignificant. The observed effect of the reaction time was expected because of the increase in the FAME content with the reaction progress. However, unlike in the present work, the increase in the reaction time over a certain limit diminished the yield of produced methyl esters [9,11,12]**.**

Interaction of the catalyst loading and the reaction time had a positive effect on the FAME content, which increased with the increase in both parameters. At the higher amounts of the catalyst the number of active sites on the catalyst surface, where the reaction occurs, is increased, thereby increasing the FAME content. This trend was observed up to about 15 % of the catalyst amount, after which the FAME content decreased, probably due to the increased viscosity of the reaction mixture and therefore aggravated mixing at higher amounts of the catalyst. Similar positive effect of the catalyst loading on the *Ceiba pentandra* oil methyl esters formation was observed in literature [9,11,12], while Betiku *et al*. [16] observed a decrease in the neem seed oil methyl esters yield with the increase in the catalyst loading and the reaction time over certain values. In the studied range of operating conditions, Betiku and Ajala [7] observed a continuous increase in the yellow oleander oil methyl esters yield with the increase in the reaction time and catalyst loading, indicating significant interactions between the two variables. Also, a high palm kernel oil methyl ester yield was reported at a prolonged reaction time independently of the catalyst amount [8].

The final hierarchical quadratic equations in terms of statistically significant actual and coded process factors, which include the insignificant reaction temperature (*A*), are as follows:

- Coded factors:

$$Y = 101.60 + 2.10A - 11.60B + 24.21D + 7.31B \cdot D - 12.55A^2 - 15.80\ B^2 - 15.86\ D^2 \tag{2}$$

- Actual factors:

$$Y = 1886.06 + 60.66A - 14.20B + 0.613D + 0.016 \cdot D - 0.502A^2 - 0{,}632\ B^2 - 0.002\ D^2 \tag{3}$$

The goodness of fit and adequacy of the developed hierarchical quadratic model was statistically assessed based on several criteria. The R^2-value of 0.811 larger than the acceptable limit of 0.80 [60] pointed out a fairly good fit of the hierarchical quadratic model that explained 81.1 % of the total variation in the FAME content, confirming the relevance to the hierarchical quadratic model for biodiesel production. The R^2_{pred}- and R^2_{adj}-values (0.789 and 0.761, respectively) differed less than the acceptable limit of 0.2 [61], confirming the good fit of the developed hierarchical quadratic model. In addition, this model had a high F_{model}-value (37.9), higher than its critical value ($F_{(0.05, 69, 70)}$ = 1.39), and a very low *p*-value (< 0.0001), implying its statistical significance of this quadratic model within the 95 % confidence level (Table 6). Furthermore, the *Adeq.Prec.*-value (24.6), which measured the signal/noise ratio for the tested system, was higher than 4, which was desirable [62], implying an adequate signal for the hierarchical quadratic model. Meanwhile, the coefficient of variation was 16 %, revealing the good precision of this model [63]. Finally, the *MRPD*-value of $\pm$14.6 (70 data) also implied the acceptability of this hierarchical quadratic model, which can be also seen in Figure S1c (Supplementary Material). Relative deviations between the predicted and actual FAME content-values in the range of 40-120 % (4 data) were observed at FAME contents lower than about 25 %; by excluding these runs from the analysis, the *MRPD*-value was reduced to $\pm$10.6 % (66 data).

The ANOVA (Table 6) showed, however, an undesirable significant lack-of-fit for this model (*p* = 0.001 < 0.050). The significant lack-of-fit meant that the variation of the replicates about their mean values was lower than the variation of the experimental points about their predicted values. A high precision of measuring the FAME content, indicated by the mean relative error between the replicates (runs 13/14, 27/28, 41/42, 55/56, and 69/70, Table S-1- Supplementary Material) of only ±1.3 %, caused a small pure error because of small deviations between the replicates [64] and hence, the significant lack of fit. This is confirmed in Figure 10, which clearly showed that the replicate experimental points are mostly above the response surface. Therefore, the significant lack of fit might refer to the existence of this systematic variation that could not be described by the hierarchical quadratic model. Since the other statistical criteria assessed

this model as a good one, its significant lack of fit, attributed to the small variance of replicated measurements, does not invalidate the model, which could be safely used for modeling and optimization the FAME content in terms of the selected process variables.

Table 6. ANOVA results for the hierarchical quadratic model including only the significant terms

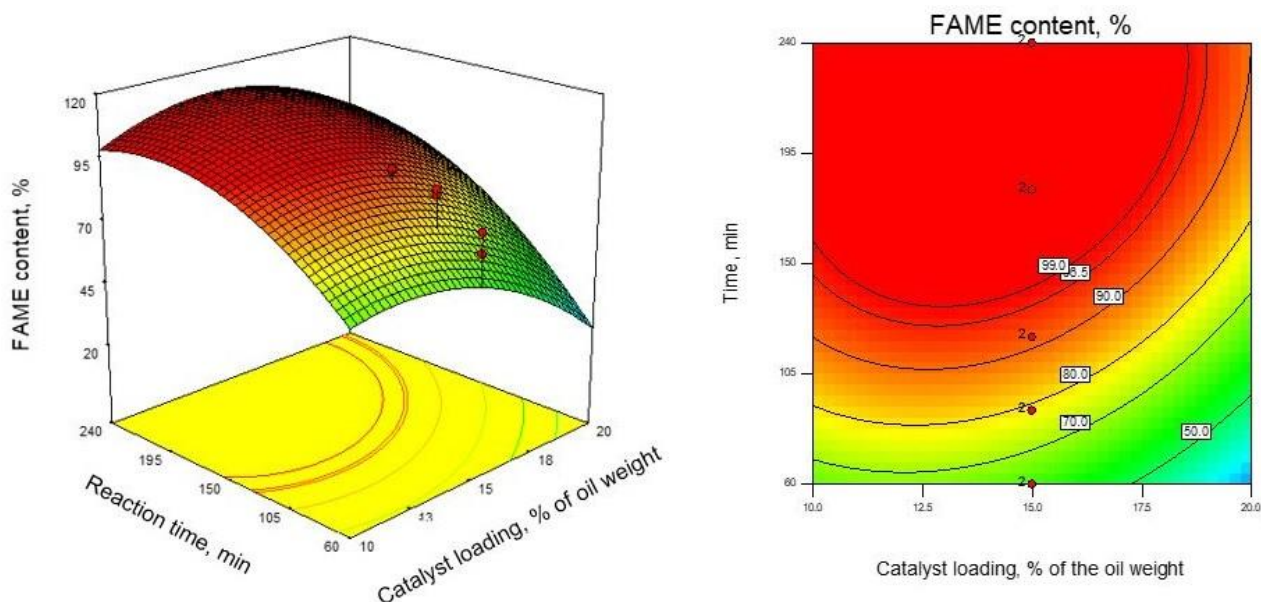| Source	Sum of squares	df	Mean square	*F*-value	*p*-value
Model	36770.1	7	5252.9	37.9	< 0.0001
A	176.8	1	176.8	1.3	0.263[a]
B	5198.9	1	5198.9	37.5	< 0.0001
D	21110.2	1	21110.2	152.3	< 0.0001
*B*x*D*	1101.7	1	1101.7	7.9	0.006
A^2	2625.0	1	2625.0	18.9	< 0.0001
B^2	4158.0	1	4158.0	30.0	< 0.0001
D^2	2813.4	1	2813.4	20.3	< 0.0001
Residual	8592.7	62	138.6		
Lack of Fit	8557.3	57	150.1	21.2	0.001
Pure Error	35.4	5	7.1		
Corrected Total	45362.8	69			

Figure 10. The response surface (a) and contour (b) plots for the FAME content as a function of catalyst loading and reaction time according to the hierarchical quadratic model (reaction temperature: 60 °C and methanol-to-oil molar ratio: 21:1)

Figure 10 shows the response surface and contour plots for the FAME content as a function of the catalyst loading and the reaction time according to the hierarchical quadratic model while keeping the reaction temperature and methanol-to-oil molar ratio constant at their medium levels (60 °C and 21:1, respectively). The FAME content increases with the progress of the reaction independently of the catalyst loading while it increases with increasing the catalyst loading until reaching a maximum at about 15 % of the oil weight and then decreases, as can be seen in Figure 10a.

The contour plot in Figure 10b shows a weak interaction between the catalyst loading and the reaction time. Besides that, it is obvious that the FAME content higher than the limit value of 96.5 % can be reached in wide ranges of the catalyst loading and reaction time, *i.e.*, for their various combinations. Also, the used software suggested several combinations of the process variables providing the targeted actual maximum FAME content of 98.6 %, as can be seen in Table S-5 (Supplementary Material). Taking the minimum methanol-to-oil molar ratio ensuring the desired FAME content as an additional criterion, the following process conditions were found to be optimum: the reaction temperature of 60.3 °C, the

catalyst loading of 11.6 % (based on the oil weight), the methanol-to-oil molar ratio of 18.3 : 1, and the reaction time of 124 min.

4. CONCLUSION

Wheat straw as waste biomass is frequently used for energy production by direct combustion, producing ash as a by-product. The fWSA catalyst, obtained by the combustion of wheat straw at open air, consists of five phases: quartz, calcite, dolomite, Mg-calcite, and sylvite. A new phase of $KHCO_3$ (hardly soluble in methanol) was detected in the aWSA sample, thus explaining its low activity. Increase in the methanolysis reaction rate with increasing the reaction temperature was observed only at the lowest methanol-to-oil molar ratio (18 : 1). The reaction rate increased with the increase in the methanol-to-oil molar ratio from 18 : 1 to 24 : 1 at the lowest catalyst loading (10 %), opposite to the highest catalyst loading of 20 %, as the result of aggravated mixing and therefore a poor contact of the liquid phase with the active sites of the catalyst. The optimum reaction conditions were found to be the reaction temperature of 60.3 ^{o}C, the catalyst loading of 11.6 % (based on the oil weight), the methanol-to-oil molar ratio of 18.3, and the reaction time of 124 min and provided the 98.6 % FAME. The fWSA catalyst showed a similarly high FAME yield as most agro-waste-based ashes having K-based active species but in longer reaction times, indicating its lower activity compared to these catalysts. Further research should focus on increasing the stability of the catalyst activity and on reducing the volume of the catalyst by compression (briquettes or pellets) or incorporation into various carriers which would facilitate the catalyst reuse.

REFERENCES

[1] Global Bioenergy Statistics 2019, World Bioenergy Association, 2019. https://worldbioenergy.org/uploads/191129%20WBA%20GBS%202019_HQ.pdf, Assessed 25.2.2021

[2] Shan R, Lua L, Shi Y, Yuan H, Shi J. Catalysts from renewable resources for biodiesel production. *Energy Convers Manage* 2018; 178: 277-289. https://doi.org/10.1016/j.enconman.2018.10.032

[3] Baskar G., I. Aberna Ebenezer Selvakumari, R. Aiswarya, Biodiesel production from castor oil using heterogeneous Ni doped ZnO nanocatalyst, *Bioresour Technol.* 2018; 250: 793-798. https://doi.org/10.1016/j.biortech.2017.12.010

[4] Veličković AV, Avramović JM, Stamenković OS, Veljković VB. Kinetics of the sunflower oil ethanolysis using CaO as catalyst. *Chem Ind Chem Eng Q.* 2016; 22: 409-418. https://doi.org/10.2298/CICEQ160106003V

[5] Nakomčić-Smaragdakis B, Čepić Z, Dragutinović N. Wheat straw combustion process and its impact on air pollution. *Cont Agric Eng.* 2014; 40: 50-62. UDK: 662.767.2:536.46

[6] Etim AO, Betiku E, Ajala SO, Olaniyi PJ, Ojumu TV. Potential of ripe plantain fruit peels as an ecofriendly catalyst for biodiesel synthesis: Optimization by artificial neural network integrated with genetic algorithm. *Sustainability*. 2018; 10: 1-15. https://doi.org/10.3390/su10030707

[7] Betiku E, Ajala SO. Modeling and optimization of *Thevetia peruviana* (yellow oleander) oil biodiesel synthesis via *Musa paradisiacal* (plantain) peels as heterogeneous base catalyst: A case of artificial neural network vs. response surface methodology. *Ind Crops Prod.* 2014; 53: 314-322. https://doi.org/10.1016/j.indcrop.2013.12.046

[8] Odude VO, Adesina AJ, Oyetunde OO., O.O. Adeyemi, N.B. Ishola, A.O. Etim, E. Betiku, Application of agricultural waste-based catalysts to trans esterification of esterified palm kernel oil into biodiesel: A case of banana fruit peel versus cocoa pod husk. *Waste Biomass Valor.* 2017; 10: 877-888. https://doi.org/10.1007/s12649-017-0152-2

[9] Betiku E, Akintunde AM, Ojumu TV. Banana peels as a biobase catalyst for fatty acid methyl esters production using napoleon's plume (*Bauhinia monandra*) seed oil: A process parameters optimization study. *Energy* 2016; 103: 797-806. https://doi.org/10.1016/j.energy.2016.02.138

[10] Gohain M, Devi A, Deka D. *Musa balbisiana* Colla peel as highly effective renewable heterogeneous base catalyst for biodiesel production. *Ind Crops Prod.* 2017; 109: 8-18. https://doi.org/10.1016/j.indcrop.2017.08.006

[11] Balaji M, Niju S. A novel biobased heterogeneous catalyst derived from *Musa acuminate* peduncle for biodiesel production – Process optimization using central composite design. *Energy Convers Manage*. 2019; 189: 118-131. https://doi.org/10.1016/j.enconman.2019.03.085

[12] Balaji M, Niju S. Banana peduncle - A green and renewable heterogeneous base catalyst for biodiesel production from *Ceiba pentandra* oil. Renewable *Energy* 2020; 146: 2255-2269. https://doi.org/10.1016/j.renene.2019.08.062

[13] Deka DC, Basumatary S. High quality biodiesel from yellow oleander (*Thevetia peruviana*) seed oil. *Biomass Bioenergy* 2011; 35: 1797-1803. https://doi.org/10.1016/j.biombioe.2011.01.007

[14] Sarma AK, Kumar P, Aslam M, Chouhan APS. Preparation and characterization of *Musa balbisiana* Colla underground stem nano-material for biodiesel production under elevated conditions. *Catal Lett.* 2014; 144: 1344-1353. https://doi.org/10.1007/s10562-014-1206-8

[15] Aslam M, Saxena P, Sarma AK. Green technology for biodiesel production from *Mesua ferrea* L. seed oil. *Energy Environ. Res.* 2014; 4 (2): 11-21. https://doi.org/10.5539/eer.v4n2p11

[16] Betiku E, Etim AO, Pereao O, Ojumu TV. Two-step conversion of neem (*Azadirachta indica*) seed oil into fatty methyl esters using a heterogeneous biomass-based catalyst: An example of cocoa pod husk. *Energy Fuels* 2017; 31: 6182-6193. https://doi.org/10.1021/acs.energyfuels.7b00604

[17] Vadery V, Narayanan BN, Ramakrishnan RM, Cherikkallinmel SK, Sugunan S, Narayanan DP, Sasidharan S. Room temperature production of jatropha biodiesel over coconut husk ash. *Energy* 2014; 70: 588-594. https://doi.org/10.1016/j.energy.2014.04.045

[18] Hindryawati N, Maniam GP, Karim MR, Chong KF. Transesterification of used cooking oil over alkali metal (Li, Na, K) supported rice husk silica as potential solid base catalyst. *Eng. Sci .Technol. Int. J.* 2014; 17: 95-103. https://doi.org/10.1016/j.jestch.2014.04.002

[19] Miladinović MR, Zdujić MV, Veljović ĐN, Krstić JB, Banković-Ilić IB, Veljković VB, Stamenković OS. Valorization of walnut shell ash as a catalyst for biodiesel production. *Renewable Energy* 2020; 147: 1033-1043. https://doi.org/10.1016/j.renene.2019.09.056

[20] Kostić MD, Bazargan A, Stamenković OS, Veljković VB, McKay G. Optimization and kinetics of sunflower oil methanolysis catalyzed by calcium oxide-based catalyst derived from palm kernel shell biochar. *Fuel* 2016; 163: 304-313. https://doi.org/10.1016/j.fuel.2015.09.042

[21] Laskar IB, Gupta R, Chatterjee S, Vanlalveni C, Rokhum L. Taming waste: Waste Mangifera indica peel as a sustainable catalyst for biodiesel production at room temperature. *Renewable Energy* 2020; 161: 207-220. https://doi.org/10.1016/j.renene.2020.07.061

[22] Mendonça IM, Paes OARL, Maia PJS, Souza MP, Almeida RA, Silva CC, Duvoisin S Jr., de Freitas FA. New heterogeneous catalyst for biodiesel production from waste tucuma peels (*Astrocaryum aculeatum* Meyer): Parameters optimization study. *Renewable Energy* 2019; 130: 103-110. https://doi.org/10.1016/j.renene.2018.06.059

[23] Uprety B.K, Chaiwong W, Ewelike C, Rakshit SK. Biodiesel production using heterogeneous catalysts including wood ash and the importance of enhancing byproduct glycerol purity. *Energy Convers. Manage.* 2016; 115: 191-199. https://doi.org/10.1016/j.enconman.2016.02.032

[24] Aleman-Ramirez JL, Moreira J, Torres-Arellano S, Longoria A, Okoye PU, Sebastian PJ. Preparation of a heterogeneous catalyst from moringa leaves as a sustainable precursor for biodiesel production. *Fuel* 2021; 284: 118983. https://doi.org/10.1016/j.fuel.2020.118983

[25] Barros S de S, Pessoa Junior WAG, Sá ISC, Takeno ML, Nobre FX, Pinheiro W, Manzato L, Iglauer S, de Freitas FA. Pineapple (*Ananás comosus*) leaves ash as a solid base catalyst for biodiesel synthesis. *Bioresour Technol.* 2020; 312: 123569. https://doi.org/10.1016/j.biortech.2020.123569

[26] Nath B, Das B, Kalita P, Basumatary S. Waste to value addition: Utilization of waste *Brassica nigra* plant derived novel green heterogeneous base catalyst for effective synthesis of biodiesel. *J Cleaner Prod.* 2019; 239: 118112. https://doi.org/10.1016/j.jclepro.2019.118112

[27] Kostić MD, Tasić MB, Đalović IG, Biberdžić MO, Mitrović PM, Stamenković OS, Veljković VB. Optimization of biodiesel production from corn oil by methanolysis catalyzed by corn cob ash. *Recycl. Sustainable Dev.* 2018; 11: 53-62. https://doi.org/10.5937/ror1801053K

[28] Vinu V, Binitha NN. Lithium silicate based catalysts prepared using arecanut husk ash for biodiesel production from used cooking oil. *Mater Today: Proc.* 2020; 25: 241-245. https://doi.org/10.1016/j.matpr.2020.01.210

[29] Changmai B, Rano R, Vanlalveni C, Rokhum L. A novel *Citrus sinensis* peel ash coated magnetic nanoparticles as an easily recoverable solid catalyst for biodiesel production. *Fuel* 2021; 286: 119447. https://doi.org/10.1016/j.fuel.2020.119447

[30] Gouran A, Aghel B, Nasirmanesh F. Biodiesel production from waste cooking oil using wheat bran ash as a sustainable biomass. *Fuel* 2021; 295: 120542. https://doi.org/10.1016/j.fuel.2021.120542

[31] Jaćimović G, Malešević M, Bogdanović D, Marinković B, Crnobarac J, Latković D, Aćin V. Wheat yield depending on long-term harvest residue incorporation. *Letopis naučnih radova* 2009; 33: 85-92. UDK: 633.11:631.82.

[32] Kim SH, Gregory JM. Straw to grain ratio equation for combine simulation. *J Biosyst Eng.* 2015; 40: 314-319. http://dx.doi.org/10.5307/JBE.2015.40.4.314

[33] Wieser H, Milijić V. Dostupnost poljoprivredne biomase u Srbiji, Deutsche Gesellschaft für Internationale Zusammenarbeit (GIZ) GmbH. Availability of agro-biomass in Serbia. 2017. http://www.bioenergy-serbia.rs/images/documents/studies/20171028_Agrobiomass_Study.pdf, Assessed January 4, 2020.

[34] Khushnood RA, Rizwan SA, Memon SA, Tulliani J-M, Ferro GA. Experimental investigation on use of wheat straw ash and bentonite in self-compacting cementitious system. *Adv. Mater. Sci. Eng.* 2014; 2014: 832508. http://dx.doi.org/10.1155/2014/832508

[35] Ahmad MR, Sharif MB, Ali HA, Hussain M, Chen B. Experimental investigation of pozzolanic concrete containing wheat straw ash. *Can. J. Civ. Eng.* 2019; 46: 941-951. https://doi.org/10.1139/cjce-2017-0419.

[36] Amin MN, Murtaza T, Shahzada K, Khan K, Adil M. Pozzolanic potential and mechanical performance of wheat straw ash incorporated sustainable concrete. *Sustainability* 2019; 11: 519. https://doi.org/10.3390/su11020519.

[37] Jankovský O, Pavlíková M, Sedmidubský D, Bouša D, Lojka M, Pokorný J, Záleská M, Pavlí Z. Study on pozzolana activity of wheat straw ash as potential admixture for blended cements. *Ceram.-Silik.* 2017; 61: 327-339. http://dx.doi.org/10.13168/cs.2017.0032

[38] Memon SA, Wahid I, Khan MK, Tanoli MA, Bimaganbetova M. Environmentally friendly utilization of wheat straw ash in cement-based composites. *Sustainability* 2018; 10: 1322. https://doi.org/10.3390/su10051322

[39] Qudoos A, Kim HG, Atta-ur-Rehman, Jeon IK, Ryou J-S. Influence of the particle size of wheat straw ash on the microstructure of the interfacial transition zone. *Powder Technol.* 2019; 352: 453-461. https://doi.org/10.1016/j.powtec.2019.05.005

[40] Sharma G, Singh K. Agro-waste ash and mineral oxides derived glass-ceramics and their interconnect study with Crofer 22 APU for SOFC application. *Ceram. Int.* 2019; 45: 20501-20508. https://doi.org/10.1016/j.ceramint.2019.07.029

[41] Bartůněk V, Sedmidubský D, Bouša D, Jankovský O. Production of pure amorphous silica from wheat straw ash. *Green Mater*. 2018; 6: 1-5. https://doi.org/10.1680/jgrma.17.00035

[42] Dodson J. Wheat straw ash and its use as a silica source. 2011; Ph. D. Thesis, Univ. York, UK, 2011.

[43] Pokorný J, Pavlíková M, Jankovský O, Łagód G, Pavlík Z. Properties of wheat straw ash geopolymer for construction use. In: Proceedings of 19th International Multidisciplinary Scientific GeoConference SGEM 2019. Sofia, Bulgary, 2019, pp. 239-246. https://doi.org/10.5593/sgem2019/6.2/S26.031

[44] Wang X, Yao K, Huang X, Chen X, Yu G, Liu H, Wang F, Fan M. Effect of CaO and biomass ash on catalytic hydrogasification behavior of coal char. *Fuel* 2019; 249: 103-111. https://doi.org/10.1016/j.fuel.2019.03.025

[45] Ali MMM, Ahmed MJ. Adsorption behavior of doxycycline antibiotic on NaY zeolite from wheat (*Triticum aestivum*) straws ash. *J. Taiwan Inst. Chem. Eng.* 2017; 81: 218-224. https://doi.org/10.1016/j.jtice.2017.10.026.

[46] Kumar A, Mandal A, Singh N. Rice and wheat straw ashes: Characterization and modeling of pretilachlor sorption kinetics and adsorption isotherm. *J. Environ. Sci. Health B* 2019; 54: 303-312. https://doi.org/10.1080/03601234.2018.1561059

[47] Trivedi NS, Kharkar RA, Mandavgane SA. Use of wheat straw combustion residues for removal of chlorinated herbicide (2,4-dichlorophenoxyacetic acid). *Waste Biomass Valor.* 2019; 10: 1323-1331. https://doi.org/10.1007/s12649-017-0134-4

[48] Đokić-Stojanović DR, Todorović ZB, Troter DZ, Stamenković OS, Veselinović LjM, Zdujić MV, Manojlović DD, Veljković VB. Triethanolamine as an efficient cosolvent for biodiesel production by CaO-catalyzed sunflower oil ethanolysis: An optimization study. *Hem. Ind.* 2019; 73: 351-362.https://doi.org/10.2298/HEMIND190822033D

[49] Stanković M, Krstić J, Gabrovska M, Radonjić V, Nikolova D, Lončarević D, Jovanović D. Supported nickel-based catalysts for partial hydrogenation of edible oils. In: *New Advances in Hydrogenation Processes - Fundamentals and Applications*. IntechOpen; 2017: https://dx.doi.org/doi.org/10.5772/66967, https://www.intechopen.com/chapters/53666

[50] Rouquerol F, Rouquerol J, Sing K. *Adsorption by Powders and Porous Solids, Principles, Methodology and Applications*. London, Academic Press; 1999.

[51] Dubinin MM. *Progress in Surface and Membrane Science.* New York, Academic Press; 1975.

[52] Barrett EP, Joyner LG, Halenda PP. The determination of pore volume and area distributions in porous substances. I. Computations from nitrogen isotherms. *J. Am. Chem. Soc.* 1951; 73: 373-380.

[53] Lecloux A, Pirard JP. The importance of standard isotherms in the analysis of adsorption isotherms for determining the porous texture of solids. *J Colloid Interface. Sci*. 1979; 70: 265-281.

[54] Veličković AV, Stamenković OS, Todorović ZB, Veljković VB. Application of the full factorial design to optimization of base-catalyzed sunflower oil ethanolysis. *Fuel* 2013; 104: 433-442. https://doi.org/10.1016/j.fuel.2012.08.015

[55] Vassilev SV, Vassileva CG, Song YC, Li WY, Feng J. Ash contents and ash forming elements of biomass and their significance for solid biofuel combustion. *Fuel* 2017; 208: 377-409. https://doi.org/10.1016/j.fuel.2017.07.036

[56] Singh B, Camps-Arbestain M, Lehmann J. Biochar: *A guide to analytical methods. Australia*, Clayton, Vic.: CSIRO Publishing; 2017.

[57] Clemente JS, Beauchemin S, Thibault Y, MacKinnon T, Smith D. Differentiating inorganics in biochars produced at commercial scale using principal component analysis. *ACS Omega 3* 2018; 6: 6931-6944. https://doi. org /10.1021/acsomega.8b00523

[58] Platonov AY, Evdokimov AN, Kurzin AV, Maiyorova HD. Solubility of Potassium Carbonate and Potassium Hydrocarbonate in Methanol. *J. Chem. Eng. Data.* 2002; 47: 1175-1176. https://doi.org/10.1021/je020012v

[59] Lôbo IP, Ferreira SLC, da Cruz RS. Biodiesel: quality parameters and analytical methods. *Quim. Nova* 2009; 32: 1596-1608. https://doi.org/10.1590/S0100-40422009000600044

[60] Lundstedt T, Seifert E, Abramo L, Thelin B, Nyström Å, Pettersen J, Bergman R. Experimental design and optimization. *Chemom. Intell. Lab. Syst.* 1998; 42: 3-40. https://doi.org/10.1016/S0169-7439(98)00065-3

[61] Anderson MJ. *Statistics Made Easy_ Blog.The DOE FAQ Alert.* 10 (6). http://www.statease.com/news/faqalert10-06.html (2020). Accessed January 8, 2020.

[62] Anderson MJ, Whitcomb PJ. RSM simplified: *Optimizing processes using response surface methods for design of experiments*. 2nd ed., New York, Productivity Press; 2005.

[63] Vaz MAB, Pacheco PS, Seidel E Jr, Ansuj AP. Classification of the coefficient of variation to variables in beef cattle experiments. *Cienc. Rural.* 2017; 47: 1-4. http://dx.doi.org/10.1590/0103-8478cr20160946

[64] Saldaña-Roblesa A, Guerra-Sánchez R, Maldonado-Rubio MI, Peralta-Hernández JM. Optimization of the operating parameters using RSM for the Fenton oxidation process and adsorption on vegetal carbon of MO solutions. *J. Ind. Eng. Chem.* 2014; 20: 848-857. https://doi.org/10.1016/j.jiec.2013.06.015

SAŽETAK

Pepeo pšenične slame kao katalizator u proizvodnji biodizela

Ana Veličković[1], Jelena Avramović[1], Milan Kostić[2], Jugoslav B. Krstić[3], Olivera Stamenković[2] i Vlada B. Veljković[2,4]

[1]Univerzitet u Prištini sa privremenim sedištem u Kosovskoj Mitrovici, Fakultet tehničkih nauka, Knjaza Miloša 7, 38220, Srbija
[2]Tehnološki fakultet, Univerzitet u Nišu, Bulevar oslobođenja, 16000 Leskovac, Srbija
[3]Institut za hemiju, tehnologiju i metalurgiju, Univerzitet u Beogradu, 11000 Beograd, Srbija
[4]Srpska Akademija nauka i umetnosti, Knez Mihailova 35, 11000 Beograd, Srbija

(Naučni rad)

Pepeo pšenične slame (PPS) je korišćen kao katalizator u proizvodnji biodizela iz sunco-kretovog ulja. Karakterizacija katalizatora je izvršena primenom metoda temperaturski programiranom razgradnjom (temperature-programmed decomposition, TPDe), rentgenskom difrakcijom (X-ray diffraction, XRD), Hg porozimetrijom, N_2 fizisorpcijom i skenirajućom elektronskom mikrosopijom sa energo-disperzivnom spektrometrijom (scanning electron microscopy and energy dispersive X-ray spectroscopy, SEM-EDS). Reakcija metanolize istraživana je pri sledećim reakcionim uslovima: temperaturni opseg 55-65 °C; količina katalizatora 10-20 % (računato na masu ulja) i opseg molskog odnosa methanol : ulje 18 : 1 – 24 : 1. Optimizacija reakcionih uslova izvršena je metodologijom površine odziva u kombinaciji sa istorijskim eksperimentalnim planom. Maksimalni prinos metil estara masnih kiselina (MEMK) od 98,6 % postignut je pri sledećim optimalnim reakcionim uslovima: temperatura 60,3 °C, količina katalizatora 11,6 % (računato na masu ulja), molski odnos methanol : ulje 18,3 : 1 i vreme trajanja reakcije 124 min. Vrednosti koeficijenata determinacije (R^2 = 0,811, R^2_{pred} = 0,789, R^2_{adj} = 0,761) i srednjeg relativnog odstupanja (±10,6 %, 66 podataka) ukazali su na prihvatljivost i pouzdanost razvijenog modela. Sadržaj MEMK nakon 4 h reakcije pri optimalnim uslovima smanjen je na 37, 12 i 3 % nakon prve, druge i treće upotrebe katalizatora, redom.

Ključne reči: agro-otpad; metil estri masnih kiselina; karakterizacija katalizatora; modelovanje; optimizacija